Climate Dynamics (2024) 62:3109–3121
https://doi.org/10.1007/s00382-023-07054-5

ORIGINAL ARTICLE

Mutual influences between ENSO and its two precursor modes in the extratropical South Pacific

Xumin Li[1] · Ruiqiang Ding[2] · Yu-Heng Tseng[3] · Jin-Yi Yu[4] · Xiaofeng Xu[1,5]

Received: 15 August 2023 / Accepted: 1 December 2023 / Published online: 5 January 2024

Abstract

The boreal spring South Pacific Oscillation (SPO) in the atmosphere and South Pacific Quadrupole (SPQ) in the ocean are recognized as significant precursors for the following winter's El Niño-Southern Oscillation (ENSO). Here we delve into the generation mechanisms of the SPO and probes the potential influence and driving forces of ENSO events on this variability mode, alongside the relationships between SPO and SPQ. Employing statistical analyses with observations spanning 1979–2021 and conducting numerical simulations, this study reveals significant correlations between the SPO and the previous-ENSO-related central tropical Pacific surface temperature anomalies (SSTAs). The forced atmospheric experiments confirm the central tropical Pacific SSTAs as an essential forcing mechanism for the SPO. A quantitative analysis further demonstrates that ENSO and atmospheric internal dynamic contribute comparably to the formation of the SPO. After the SPO formation, it influences the underlying ocean, generating the SPQ mode. Investigations with coupled numerical experiments show the induced SPQ can trigger 46.6% of the original neutral events into El Niño events. This study identifies and validates the sequence of physical processes linking SPO and SPQ to ENSO. The findings highlight the existence of loop-like mutual influence processes between ENSO and the two extratropical variability modes (SPO and SPQ) in the South Pacific. This cyclic pattern bears significant implications for understanding the temporal development of ENSO and can fortify ENSO predictability.

Keywords ENSO prediction · South Pacific oscillation · South Pacific quadrupole · Mutual influence · Central tropical Pacific SSTAs · Atmospheric internal dynamic

1 Introduction

El Niño-Southern Oscillation (ENSO) emerges as the tropical Pacific's leading orchestrator of year-to-year climate variations (McPhaden et al. 2006). Due to its widespread influences on global climate, marine ecosystems, and human activities (Timmermann et al. 2018), extensive research focused on ENSO prediction (Tseng et al. 2017; Tang et al. 2018). Historically, the ENSO prediction community primarily focused on local tropical Pacific precursors, such as Warm Water Volume (Jin 1997a, b), Westerly Wind Events (McPhaden et al. 1992; Fedorov et al. 2015), and Madden-Julia Oscillation (Madden and Julian 1994; Hendon et al. 2007).

However, considering only these tropical precursors is not sufficient for ENSO prediction. Illustratively, the attenuated El Niño event of 2014/2015 experienced an unexpected pause during the boreal summer of 2014, despite initial predictions of a wintertime super El Niño by most real-time

✉ Ruiqiang Ding
drq@bnu.edu.cn

✉ Xiaofeng Xu
xiaofeng_x@hotmail.com

1 Key Laboratory of Meteorological Disaster of Ministry of Education (KLME), Nanjing University of Information Science and Technology, Nanjing, China

2 Key Laboratory of Environmental Change and Natural Disasters of Chinese Ministry of Education, Beijing Normal University, Beijing, China

3 Institute of Oceanography, National Taiwan University, Taipei, Taiwan

4 Department of Earth System Science, University of California, Irvine, CA 92697, USA

5 China Meteorological Administration Training Center, Beijing, China

forecast models. An unusual decrease in sea surface temperatures (SSTs) in the southeastern subtropical Pacific region was likely the cause of this unexpected cessation, as illuminated by further research (Zhu et al. 2016; Ding et al. 2017; Ineson et al. 2018). This event underscores that climate variability from the extratropics could play a potential role in ENSO prediction.

There were increasing studies on extratropical precursors for ENSO, particularly those from the North Pacific. Among these precursors, the North Pacific Oscillation (NPO) stands out, having been studied extensively (Rogers 1981; Anderson 2003). Additionally, oceanic modes forced by the NPO, namely the North Pacific Meridional Mode (NPMM) (Chiang and Vimont 2004; Chang et al. 2007) and Victoria Mode (VM) (Bond et al. 2003; Ding et al. 2015a), have been recognized as potent triggers for ENSO. These phenomena exert their influence through intricate mechanisms like the thermodynamic seasonal footprinting (Vimont et al. 2001, 2003a, b; Ding et al. 2015a) and the dynamic trade wind charge (Anderson 2004; Anderson et al. 2013), primarily commencing in the boreal spring season.

Correspondingly, the vast and adjacent South Pacific might also hold a role in exerting considerable influence on ENSO development. Several studies underlined the unique contribution of South Pacific climate variability in ENSO prediction, even though it was not as thoroughly examined as the North Pacific. As illustrated by You and Furtado (2017), a notable example is the South Pacific Oscillation (SPO), recognized as a meridional dipole in sea level pressure (SLP) variability over the South Pacific region. This phenomenon was found to greatly impact ENSO intensity six months later. Additionally, research indicated that as early as boreal spring, SLP anomalies (SLPAs) over the South Pacific can serve as effective precursors for subsequent El Niño occurrences. Further examination revealed that this boreal spring SLPA structure in boreal spring is precisely the preceding pattern of the SPO (Min and Zhang 2020).

In the oceanic fields, Ding et al. (2015b) identified a South Pacific Quadrupole (SPQ) mode of SST variability as an additional precursor for ENSO. The SPQ and ENSO demonstrate the closest correlation when the SPQ precedes ENSO by a nine-month period. Over the southeastern Pacific, there exists South Pacific Meridional Mode (SPMM) and it was shown to be effective in facilitating the development of subsequent ENSO events (Zhang et al. 2014). Moreover, by contrasting the predictive capacities of SPQ and SPMM, it is concluded that the SPQ demonstrates a more robust linkage to ENSO than does SPMM (Ding et al. 2020). The privilege of the SPQ is attributed to its unique structure, which encompasses an additional element of SSTAs, found not only in the southwest Pacific but also extending into the high-latitude South Pacific. Therefore, the current study will concentrate on the basin-scale SPQ rather than the SPMM, as the investigation aims to elucidate the connection between the most effective South Pacific ENSO precursor and ENSO itself.

However, the origins of these south Pacific ENSO precursors (i.e., the SPO in the atmosphere and the SPQ in the ocean) are still under debate. Regarding the origins of the SPO, You and Furtado (2017, 2019) emphasized that the SPO is more influenced by atmospheric internal variability than by simultaneous developing ENSO. Their studies, however, were primarily focused on the boreal summer season, when the ENSO event is often already underway. Later, as for the boreal spring ENSO precursor in the atmosphere, Min and Zhang (2020) decomposed South Pacific SLPAs and revealed that the boreal spring ENSO precursor can be seen as the combination of two empirical orthogonal function (EOF) modes. While their focused season was boreal spring, they did not explore the external forcing that responsible for the SPO. Therefore, an important question arises: what is the external forcing behind the boreal spring SPO? Can tropical Pacific SSTAs act as a forcing mechanism for the boreal spring SPO? If so, how do they compare with atmospheric internal variability in steering the variability of the boreal spring SPO?

As for the origin of the oceanic SPQ, Ding et al. (2015b) suggested that the SPQ is primarily forced by the one-month earlier Pacific-South-American-like (Mo and Higgins 1998) atmospheric variability. What's noteworthy is that the preceding SLPA pattern correlated with the SPQ (their Fig. 1a) exhibits a strong resemblance to the later-identified SPO pattern. Zheng and Wang (2017) replicated the SPQ structure using a singular vector decomposition method applied to SST and wind field (their Fig. 1a), uncovering a meridional dipole pattern that is in alignment with the SPO pattern. Therefore, it is imperative to investigate the exact mode preceding the SPQ, is it indeed the SPO? If so, how does the SPO-forced SPQ facilitate subsequent ENSO events? While previous studies have explored the foundational physical processes through observational data, validation using advanced numerical models is warranted to corroborate the role of SPQ in facilitating following ENSO. Additionally, what is the extent to which the SPQ contributes to the evolution of subsequent ENSO occurrences?

In this research, the focus is set on examining the reciprocal interplay between ENSO and its two extratropical South Pacific precursors, namely the SPO in the atmosphere and SPQ in the ocean. Not only atmospheric general circulation model (AGCM) but also coupled general circulation model (CGCM) experiments are conducted to investigate their interactions. Section 2 describes the specific reanalysis datasets, indices, and climate models utilized in this research. In Sect. 3.1, a detailed analysis is conducted to explore the influence of tropical Pacific heat anomalies in forcing the variation of the SPO. Section 3.2 contrasts the contributions of tropical Pacific SSTs

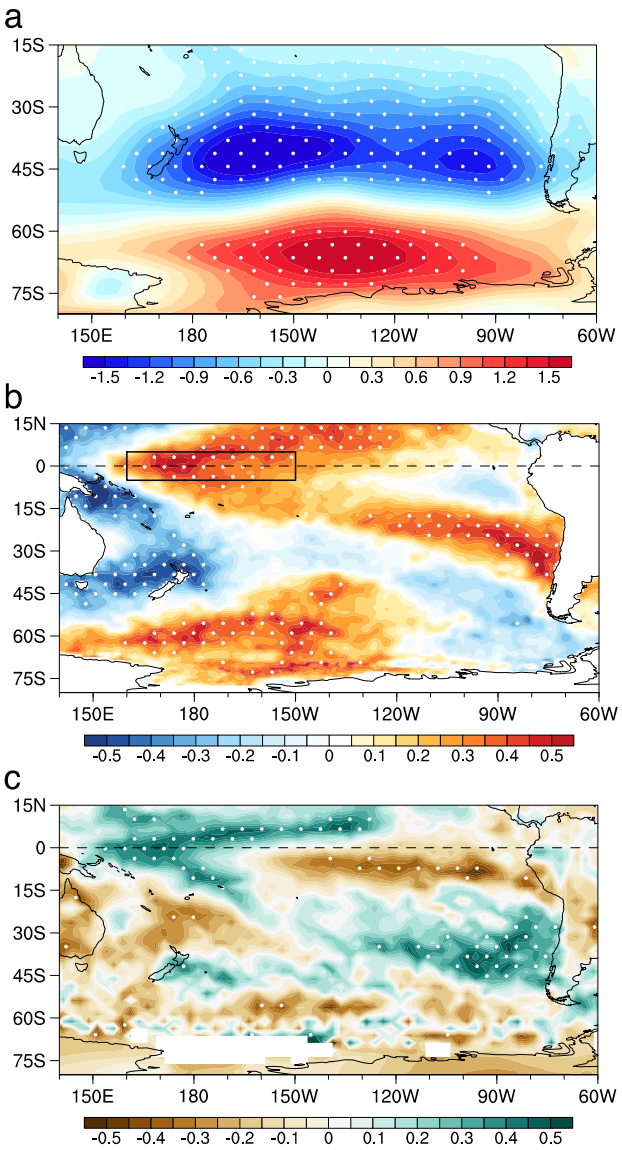

Fig. 1 **a** Regressions of FMA0 SLPAs (shading; hPa) onto the simultaneous SPO index. **b** Correlation maps between FMA0 tropical Pacific SSTAs and the SPO index, with the Niño4 region delineated by a black box. **c** Correlation maps of FMA0 tropical Pacific precipitation anomalies with the SPO index. In (**a**–**c**), white dots indicate regressions or correlations that are statistically significant at the 90% confidence level

with atmospheric internal variability in generating the SPO. Section 3.3 encompasses a sensitivity experiment to verify the efficiency of SPQ in inducing subsequent ENSO. Finally, Sect. 4 gives the summary and discussion.

2 Data and methodology

2.1 Reanalysis data

Global SST data employed here is derived from the Hadley Center Global Sea Ice and Sea Surface Temperature (HadISST) dataset, known for its detailed 1° by 1° resolution (Rayner et al. 2003). Wind and SLP data are sourced from the National Centers for Environmental Prediction and the National Center for Atmospheric Research (NCEP-NCAR) (Kalnay et al. 1996). Precipitation data is obtained from the Climate Prediction Center Merged Analysis of Precipitation (CMAP) (Xie and Arkin 1997). In here, we focus on the years 1979 to 2021. To make sure the findings are accurate, we used a two-tailed Student's *t* test for the statistics.

2.2 Indices

According to the key region of the boreal spring SPO pattern (see the Fig. 2a in You and Furtado 2017), the SPO index's determination is grounded in the average SLPAs over 46°S–27°S and 165°E–82°W. Here, we focus on the northern node of the SPO as it has the most important linkages with the following ENSO events (You and Furtado 2019). Furthermore, the definition of the Niño4 index is founded upon the area-averaged SSTAs within the coordinates of 5°S–5°N and 160°E–150°W, while the Niño3.4 index shares similar premises but is constrained to the boundaries of 5°S–5°N and 170°–120°W. The calculation of the SPQ index is performed by taking the total of the normalized SSTAs over two positive poles, located within the coordinates of [58°–36°S, 173°–145°W] and [37°–17°S, 103°–76°W], and then subtracting the aggregate of the normalized SSTAs over two corresponding negative poles, defined by the regions [47°–25°S, 142°E–179°W] and [59°–40°S, 113°–81°W].

2.3 Numerical models

Utilizing the Geophysical Fluid Dynamics Laboratory Atmospheric Model version 2.1 (hereafter GFDL; Delworth et al. 2006), two distinct AGCM experiment sets are conducted. With the implementation of a spatial configuration marked by 2.5° longitude and 2° latitude horizontal resolution and an architectural composition of 24 vertical strata, the GFDL model is primed to illuminate the intricacies of atmospheric dynamics. By focusing on the atmospheric dynamics, these simulations can help unravel how changes in the tropical Pacific SSTs project into altered patterns of the SPO.

To validate the distinctive role of SPQ in promoting ENSO events, a set of CGCM experiment was conducted

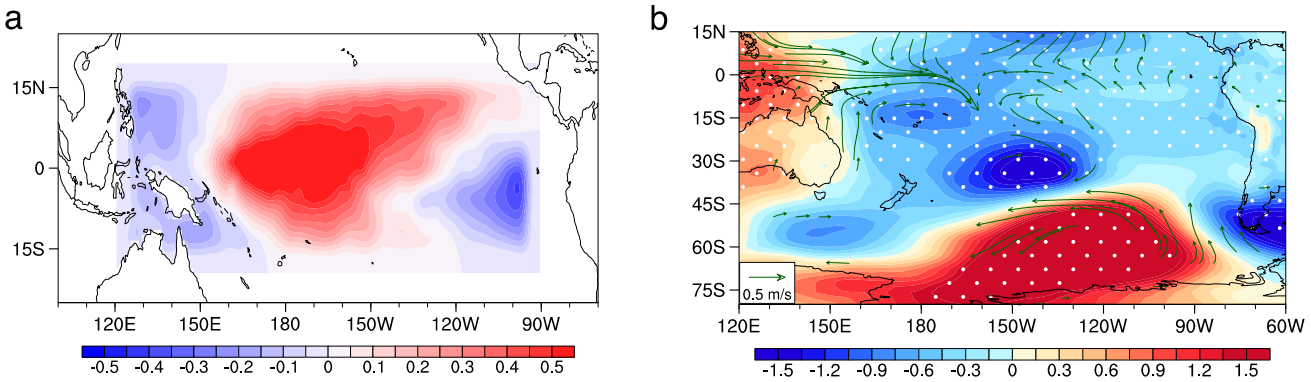

Fig. 2 **a** Prescribed SSTAs (°C) over 20°S–20°N and 120°E–90°W in February, March, and April for the ENSO-FORCE experiment. **b** Ensemble mean response of SLP (shading; hPa) and 10 m winds (vectors; m s^{-1}) in the ENSO-FORCE experiment, compared to that of the CTRL experiment. White dots represent significant SLPAs with a confidence level of 90%

with the Community Earth System Model version 1.2.2.1 (hereafter CESM). Developed at the NCAR and documented by Hurrell et al. (2013), CESM stands as a robust platform for comprehensive Earth system simulations. Extensive research has shown its ability to reasonably simulate ENSO events, including their periodicity, magnitude, and asymmetry (DiNezio et al. 2017; Wieners et al. 2019).

3 Results

3.1 The forcing role of central tropical Pacific SSTAs to SPO

The SPO manifests as a dipolar structure of SLPAs, which has opposite polarities of anomalies between a high-latitude center and a subtropical center (You and Furtado 2017). During the boreal spring, the positive phase of the SPO exhibits a negative anomaly center around 42°S and a positive anomaly center around 66°S (Fig. 1a), a pattern discerned through the regression of SLPAs against the SPO index. This spatial pattern echoes the SPO structure delineated by You and Furtado (2017; their Fig. 1a). An exploration of the link between the February–March–April (FMA0, '0' refers to the first year) SPO index and simultaneous tropical Pacific SSTs reveals significant positive correlations in the western-central tropical Pacific and corresponding negative ones over the Maritime Continent (Fig. 1b). The area of most pronounced correlation coincides with the Niño4 region, underscoring the intimate association of the SPO's positive (negative) phase with El Niño (La Niña) phenomena. We then used the Niño4 index to represent ENSO activities and find the index to have a 0.41 correlation (significant at the 99% confidence level) with the SPO index in FMA0 during 1979–2021. This statistical analysis suggests that boreal spring central tropical Pacific SSTs has a close relationship with simultaneous South Pacific atmospheric variability. The correlation map between the precipitation anomalies over tropical Pacific and the SPO index also shows a significant precipitation enhancement west of the dateline (Fig. 1c). This pattern implies that the central tropical Pacific SST variations can induce precipitation anomalies (therefore anomalous heating to the atmosphere) to possibly force SLP variation in the Southern Hemisphere, leading to a SLP variability mode like SPO.

To substantiate the driving role of central tropical Pacific SSTAs on SPO variability, a series of forced atmosphere experiments was carried out using the GFDL model. The first set of the experiments includes a control experiment (CTRL) and a sensitivity experiment (ENSO-FORCE). In the CTRL experiment, monthly varying climatological SSTs were prescribed to force the AGCM. In the ENSO-FORCE experiment, monthly El Niño SSTAs across the tropical Pacific were added to the climatological SSTs to force the AGCM. The designated area spans from 20°S to 20°N in latitude and from 120°E to 90°W in longitude, including a surrounding 5° buffer zone. We first removed the Niño3-related SSTAs from the tropical Pacific SSTA field to exclude the influence from eastern tropical Pacific. Then the residual tropical Pacific SSTAs were regressed onto the Niño4 index to produce the El Niño SSTAs (Fig. 2a). As for the 5° buffer zone, we initially only prescribed the observed SSTAs to a smaller area (15°S–15°N and 125°E–95°W) within this forcing domain. SSTAs are set to zero outside this area. We then implemented a 9-point spatial smoothing across the global grid. This procedure extended the effective SSTA forcing domain outside the initial SST prescription area by 1 degree (given a resolution of 1°×1°), adjusting the prescription area to 16°S–16°N, 124°E–94°W. After repeating this spatial smoothing procedure four more times, the forcing domain ultimately reached an area bounded by 20°S–20°N and 120°E–90°W. This smoothing procedure

effectively created a 5° buffer zone within the final forcing area. The same method was used to establish a 5° buffer zone for the SST forcing areas used in the HIST and SPQ-FORCE experiments. The El Niño SSTAs were added to the climatological SSTs in February, March, and April. The forcing continued to rely on the climatological SSTs in rest months. Both CTRL and ENSO-FORCE simulations were run for 40 years, but the analysis only focused on the last 30 years to avoid initial spin-up biases.

Figure 2b displays the differences in simulated SLP and 10-m winds between the ensemble means of ENSO-FORCE and CTRL. The simulated SLP difference pattern exhibits a negative northern node around 35°S and 145°W and a positive southern node around 60°S and 120°W, resembling the observed SPO pattern. The simulated results suggest that an atmospheric teleconnection from central tropical Pacific warming can drive the SPO pattern in the Southern Hemisphere.

Subsequently, another set of forced AGCM experiment (HIST) was conducted to explore the extent to which the interannual fluctuations of SPO are driven by the corresponding variations in tropical Pacific SSTs on an interannual scale. In this HIST experiment, the observed monthly SSTAs during 1979–2018 were integrated with the climatological SSTs within the specified boundary (20°S to 20°N latitude and 140°E to 90°W longitude). While other region was forced only by the monthly climatological SSTs. Hence, the variability of the simulated SPO is solely ascribable to the SSTAs confined to the tropical Pacific, excluding those in other regions. This experiment was also performed with 30 ensembles with slightly different initial SST fields. Following the definition in observation, the SPO index in simulation was calculated. The ensemble-mean SPO index (black line in Fig. 3), along with its standard deviation (SD; grey shading in Fig. 3), reveals strong connections with the Niño4 index. This connection is evidenced by significant correlation coefficient (R = 0.84, significant at 99% confidence level) and high sign consistency rate (75%). Following Le and Bae (2019), we conducted causal analysis on Niño4 and ensemble-mean SPO indices and revealed that there is minimal probability that Niño4 has no causal connection to SPO. Power spectrums of Niño4, observed SPOI, ensemble-mean SPOI all predominantly display periods close to 5 years (Fig. 3b). All these analyses confirm that the variations in the simulated SPO are indeed a substantial response to the alterations in tropical Pacific SSTAs. Additionally, ensemble-mean SPO index exhibits a noteworthy correlation coefficient (R = 0.42; significant at 99% confidence level) with observed SPO index. This finding lends support to the assertion that the variability observed in the SPO can be partially attributed to the variations in tropical Pacific SSTs.

3.2 Relative contributions of central tropical Pacific SSTAs and atmospheric internal variability to SPO

The findings detailed above elucidate that the SPO is subject to influence from simultaneous tropical Pacific SST variability, especially those in the central tropical Pacific. Nevertheless, certain aspects of SPO's variability remain enigmatic and cannot be solely attributed to a forced response to central tropical Pacific SSTs. To investigate the internal variability part of the SPO, we removed the simultaneous Niño4 regressions from the SLP field and then performed an EOF analysis with the residual SLPAs during the FMA0 season. The resulting EOF1 pattern (Fig. 4a) still resembles a SPO pattern, and its pattern correlation coefficient with Fig. 1a is 0.83. The associated principal component (PC1) exhibits a correlation of 0.50 (significant at the 99% confidence level; Fig. 4b) with the raw SPO index. Therefore,

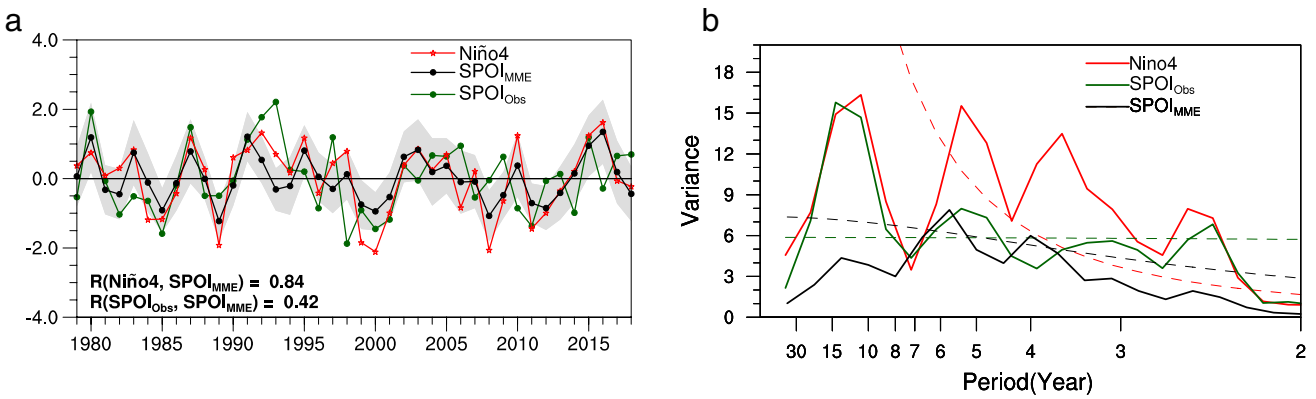

Fig. 3 **a** Red and green lines represent the observed Niño4 and SPO indices, respectively. Black line denotes the 30-member ensemble mean in HIST experiment and is superimposed by one standard deviation (gray shading). Correlation coefficients (R) between these indices are also shown. **b** Power spectrums of Niño4 (red solid line), SPO (green solid line) and ensemble-mean SPO indices (red solid line). Dashed lines denote the 90% confidence level for red noise

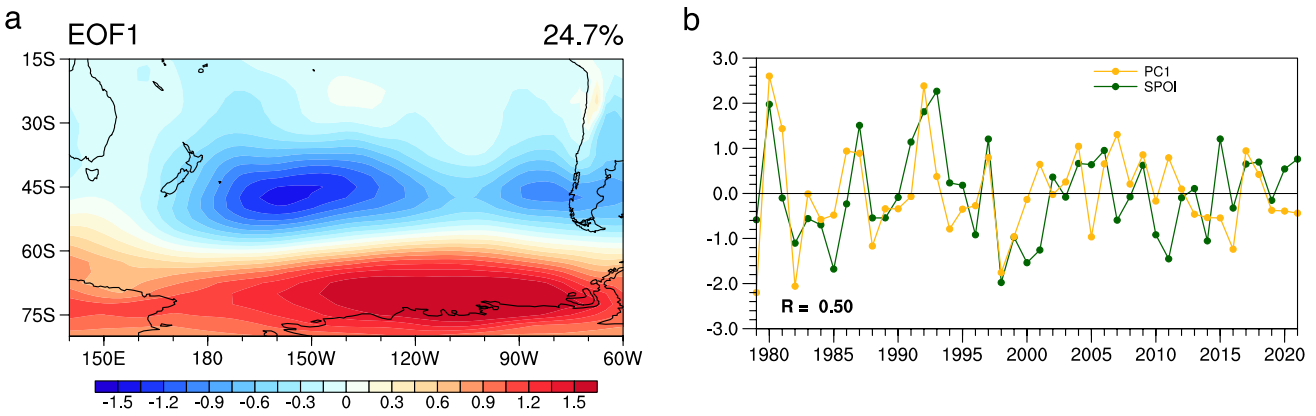

Fig. 4 **a** EOF1 spatial pattern for residual FMA0 SLPAs in the South Pacific (80°S–15°N, 140°E–60°W), after linearly removing the simultaneous tropical Pacific signal, accounting for 24.7% of the total variance. **b** Time series of PC1 associated with EOF1 and the original SPO index, along with the correlation coefficient, indicating the statistical relationship between PC1 and the SPO index

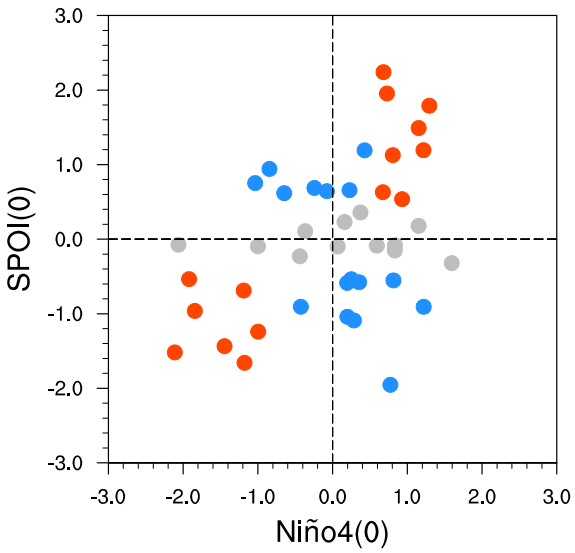

Fig. 5 Scatterplot of FMA0 Niño4 index against SPO index. Red dots denote SPO events with a positive central tropical Pacific SSTAs contribution, blue dots denote SPO events with a negative central tropical Pacific SSTAs contribution, and gray dots represent years with a SPO index too weak to be recognized as SPO events

besides the evident forced variability associated with central tropical Pacific SSTAs, the SPO also exhibits high internal variability.

We next investigated the relative influences of central tropical Pacific SSTs and the South Pacific atmospheric internal variability in shaping the SPO. To address this question, we examined the SPO and ENSO (represented by the Niño4 index) for each year to determine how many SPO events are accompanied with significant central tropical Pacific SST warming/cooling and how many are not. Here we adopt a threshold of 0.5 SD to categorize SPO events (|SPO index|> 0.5 SD; blue and red dots in Fig. 5), effectively excluding weak events (|SPO index|≤ 0.5 SD; grey dots in Fig. 5).

For those SPO events with a magnitude larger than ± 0.5 SD in FMA0, they are classified into four categories based on their accompanying Niño4 index conditions (Table 1). Among the 14 events of strong positive SPO, eight of them (57%) are accompanied by Niño4 values larger than 0.5 SD, signifying a contributory role played by the El Niño. Constantly, the remaining six instances (43%) occurred without significant positive SSTAs over central tropical

Table 1 Classification of historical SPO events based on combinations of SPO and Niño4 phases

Classification	Year	Proportion (%)
SPOI > 0.5& Niño4 > 0.5	1980, 1987, 1991, 1992, 1993, 2005, 2015, 2020	53
SPOI > 0.5& Niño4 > 0.5	1997, 2004, 2006, 2009, 2017, 2018, 2021	47
SPOI < – 0.5& Niño4 < – 0.5	1984, 1985, 1989, 1999, 2000, 2001, 2011	44
SPOI < – 0.5& Niño4 < – 0.5	1979, 1982, 1983, 1988, 1996, 1998, 2007, 2010, 2014	56

Events are included only if the SPO index magnitude exceeds 0.5 standard deviations

Pacific (Niño4 < 0.5 SD). For the 13 events of large negative phase of the SPO, six of them (46%) are synchronized with a strong La Niña (i.e., Niño4 values less than –0.5 SD), whereas the other seven of them (54%) coincided with modest central tropical Pacific SSTAs (Niño4 values above –0.5 SD). Remarkably, both the positive SPO events influenced by conducive El Niño-related central tropical Pacific SSTAs (red dots; Fig. 5) and negative SPO events shaped by corresponding La Niña-related central tropical Pacific SSTAs (blue dots; Fig. 5) occur in roughly equal proportions, each around 50%. Overall, our analyses in this section indicate that for the SPO events, approximately half manifest a close alignment with central tropical Pacific SSTs, with the remainder attributable to intrinsic variability. The formation of SPO is shaped through an intricate balance, with contributions not only from the dynamics observed within central tropical Pacific SSTs but also from the complexities related to internal variability in the extratropical atmosphere.

Following Hu et al. (2019), the signal-to-ratio method was also employed to examine the relative contributions of SST forcing and atmospheric internal variability in the variability of boreal spring South Pacific Oscillation. Here, the signal refers to as the SD of the ensemble-mean SPOI in FMA0, denoted by σ_{signal}, while the ensemble model spread, representing the noise, is defined as the SD of individual simulation members from the ensemble-mean SPOI, denoted as σ_{noise}. For simulated variable $F_{m,n}$ with ensemble member m and year n,

$$\sigma_{noise} = \left[\frac{1}{(M-1)(N-1)} * \sum_{n=1}^{n=N} \sum_{m=1}^{m=M} (F_{m,n} - \overline{F}_n)^2 \right]^{0.5},$$

$$\sigma_{signal} = \left[\frac{1}{(N-1)} * \sum_{n=1}^{n=N} (\overline{F}_n - \overline{F})^2 \right]^{0.5},$$

$$\overline{F}_n = \frac{1}{M-1} \sum_{m=1}^{m=M} F_{m,n},$$

$$\overline{F} = \frac{1}{(M-1)(N-1)} \sum_{n=1}^{n=N} \sum_{m=1}^{m=M} F_{m,n},$$

$$SNR = \frac{\sigma_{signal}}{\sigma_{noise}},$$

where $M = 30$ (total ensemble members) and $N = 40$ (years).

The SD of the ensemble-mean SPOI (i.e., σ_{signal}) is 0.67 (red bar in Fig. 6). Meanwhile, the SD of individual simulation members from the ensemble-mean SPOI (i.e., σ_{noise}) is 0.79 (grey bar in Fig. 6). A resulting SNR is 0.85, which indicates the substantial role played by tropical SST forcing in SPO variability and is almost on par with the influence of atmospheric internal variability.

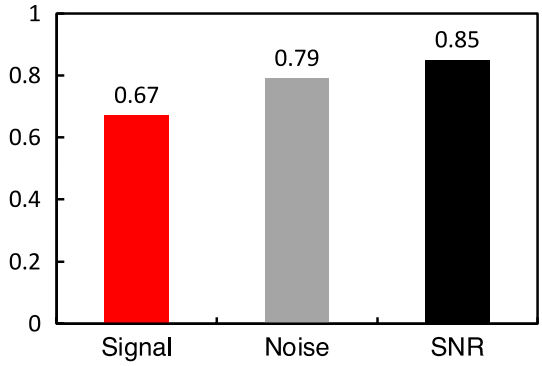

Fig. 6 Standard deviation of the ensemble-mean SPOI (red bar) and the standard deviation of individual simulation members relative to the ensemble-mean SPOI (gray bar) based on HIST outputs, which indicate signal and noise, respectively. Black bar indicates the signal-to-noise ratio

3.3 The influence of SPO/SPQ on following ENSO

The abovementioned results have revealed the influences from tropical ENSO to extratropical SPO, the next question is how the SPO affects subsequent ENSO. As mentioned earlier, there is a strong likelihood that the SPO initially drives the underlying ocean to generate the SPQ through surface heat fluxes (Ding et al. 2015b), and then through air-sea interaction across the extratropical South Pacific, gradually transfers the anomaly signal equatorward, thereby invoking Bjerknes feedback (Bjerknes 1969) and triggering the ENSO event. Figure 7a uncovers a peak correlation (R = 0.34; significant at the 99% confidence level) when the monthly atmospheric SPO index precedes the oceanic SPQ index by a single month. Additionally, the FMA0 SPO index exhibits the highest correlation (R = 0.57; significant at 99% confidence level) with the SPQ index in MAM0 (March–April–May), rather than with other seasons (Fig. 7b). Furthermore, the distribution of SSTAs related to SPO (Fig. 1b) closely resembles the distribution of SSTAs related to SPQ (Fig. 8a). Both SSTA fields (Figs. 1b and 8a) exhibit two positive SSTA centers over the Tasman Sea near the southeast Australian coastline and proximate to the Bellingshausen Sea, along with two negative SSTA center over the Ross Sea and off the west coast of Chile. Hence, we can conclude that the oceanic mode forced by the SPO is indeed the SPQ, or alternatively, the atmospheric-driven mode of the SPQ is the SPO.

Several studies have illustrated the mechanisms through which how boreal winter ENSO events are influenced by

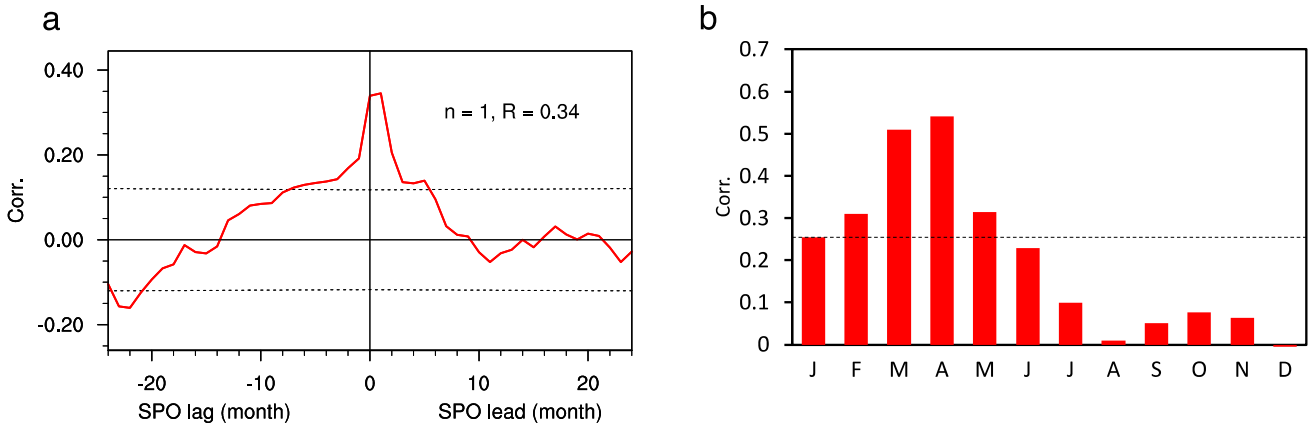

Fig. 7 **a** Lead-lag relationships between the monthly SPO and SPQ indices, including the timing and magnitude of the peak correlation. **b** Correlation coefficients for the FMA0 SPO index with the SPQ index across various months. Horizonal dashed lines in both (**a**) and (**b**) denote the 90% confidence threshold

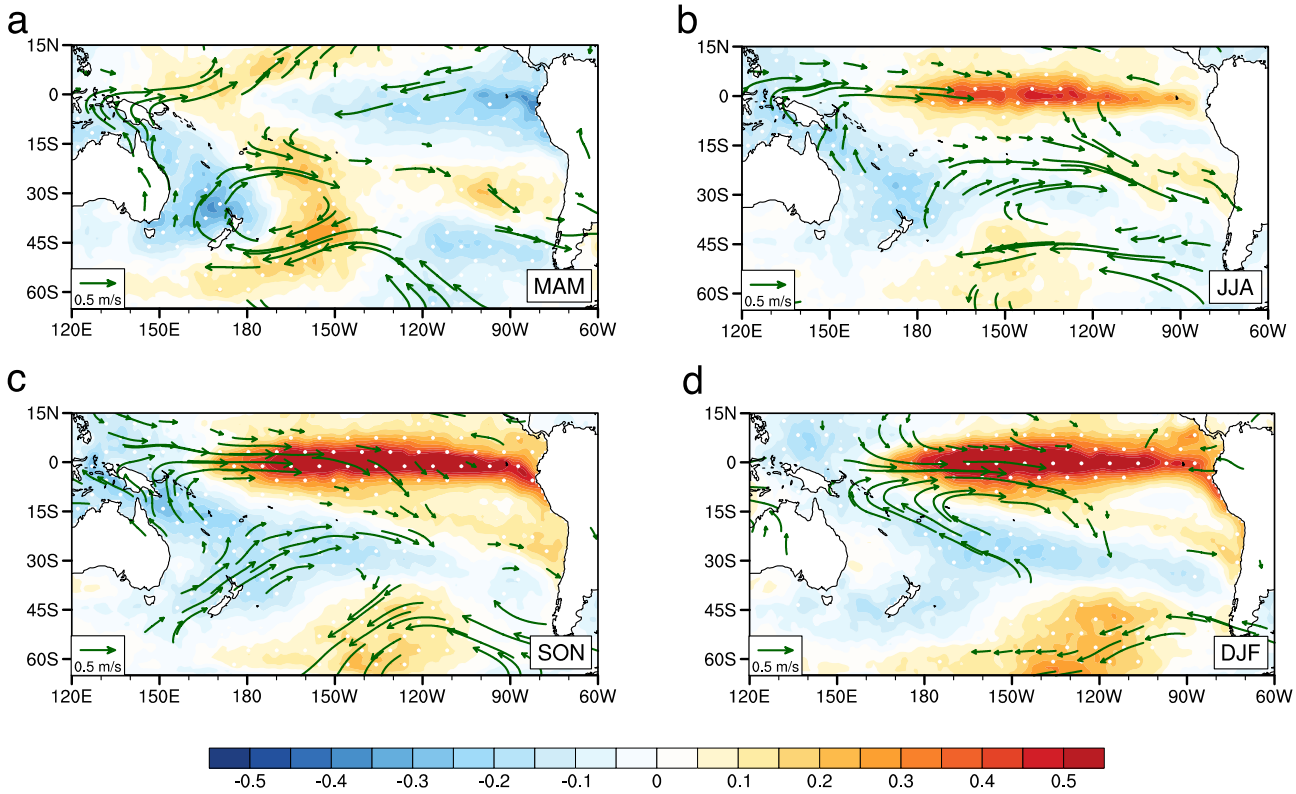

Fig. 8 **a**–**d** Regressions of observed SSTAs (shading; °C) and 850 hPa wind anomalies (vector; m s^{-1}) for **a** MAM0, **b** JJA0, **c** SON0, and **d** D0JF1, against the MAM0 SPQ index. Areas with stippling indicate regions of statistical significance at the 90% confidence level, and wind vectors exceeding the 90% confidence threshold are displayed

the boreal spring SPQ (Ding et al. 2015b; Li et al. 2020). The SPQ was shown to lead to anomalous cold (warm) water in the southwest (southeast) Pacific, along with overlaying wind anomalies. These anomalies maintain and enhance each other, and through positive Wind-Evaporation-SST (WES) feedbacks (Xie and Philander 1994), they extend equatorward into the western-central (central-eastern) Pacific. This extension strengthens the equatorial Pacific anomalous westerlies and further cultivates equatorial Pacific warming through the well-known Bjerknes feedback during the subsequent summer and autumn (June–July–August, JJA0; September–October–November,

SON0; respectively) (Fig. 8b and c). By the following winter (D0JF1), significant positive SSTAs, that is an El Niño, are fully developed in the equatorial Pacific (Fig. 8d).

However, the distinctive role of SPQ in facilitating ENSO event has yet to be verified within climate models. Here, a suite of sensitivity experiments were conducted using the CESM, aimed at validating whether the trigger role of SPQ in following ENSO events can be replicated in an advanced climate model. This experiment was conducted in three steps. First, we let the CESM model freely integrate for 120 years under preindustrial (1850) radiative forcing condition. Second, we selected ENSO-neutral years from the 120 years control simulation, ensuring the simulated Niño3.4 index in D0JF1 lay within ± 0.5 °C range, thus identifying 30 ENSO-neutral years for what was termed the CTRL simulation. Third, a 30-member sensitivity experiment called the SPQ-FORCE simulation was conducted. The initial state for each ensemble member was extracted from the January 1st status of the 30 identified ENSO-neutral years. The SSTs during March–June over the SPQ region (65°S–10°S and 130°E–70°W, with a 5° buffer zone; Fig. 9) is nudged toward the SPQ-related SSTAs plus the climatological SSTs. The SPQ-related SSTAs during March–June was constructed by regressing the corresponding $4 \times$SSTAs onto the MAM0 SPQ index. Each ensemble member is integrated from January to second year February, for a total of 14 months. It is important to note that this experiment has been designed to exclude those years predisposed to develop into ENSO, guaranteeing the absence of any precursors in initial field that might culminate in a mature ENSO event. This approach allows for a clear attribution of any substantial shifts in SSTs over the tropical Pacific in D0JF1 solely to the externally imposed forcing, specifically the SPQ-related SSTAs.

The ensemble-mean discrepancies between SPQ-FORCE and CTRL, as depicted in Fig. 10a–d, reveal insights into the SPQ's influence on ENSO. Initially, the simulation shows an absence of distinct SSTA indicators within the tropical Pacific (Fig. 10a). This eliminates the likelihood that any pre-existing tropical SSTAs contribute to an ENSO event

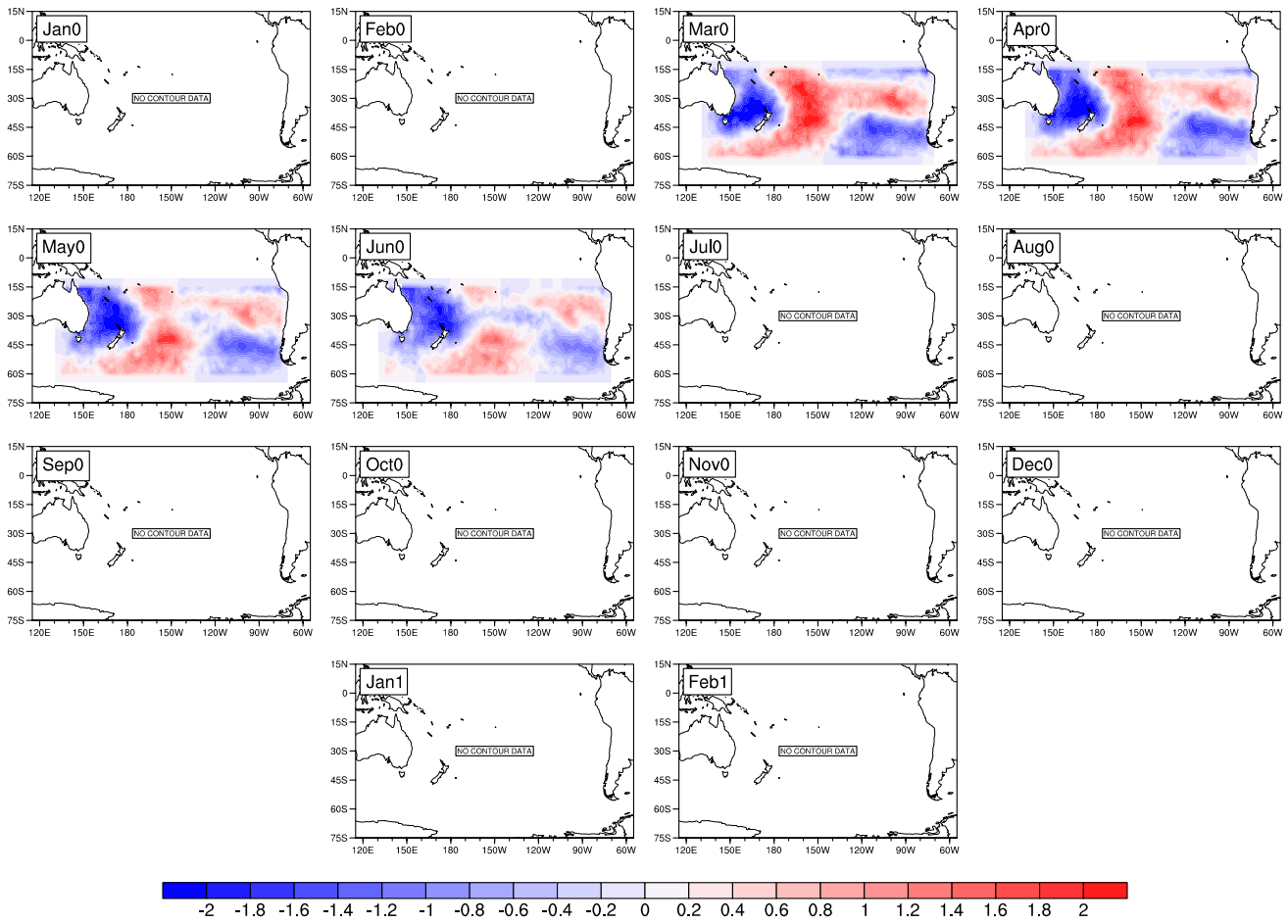

Fig. 9 Prescribed SSTAs (65°S–10°S and 130°E–70°W; °C) from Jan0 to Feb1 for the SPQ-FORCE experiment in the fully coupled CESM. Only the shaded areas are forced by SPQ-related SSTAs (°C), while the remaining regions are set to zero

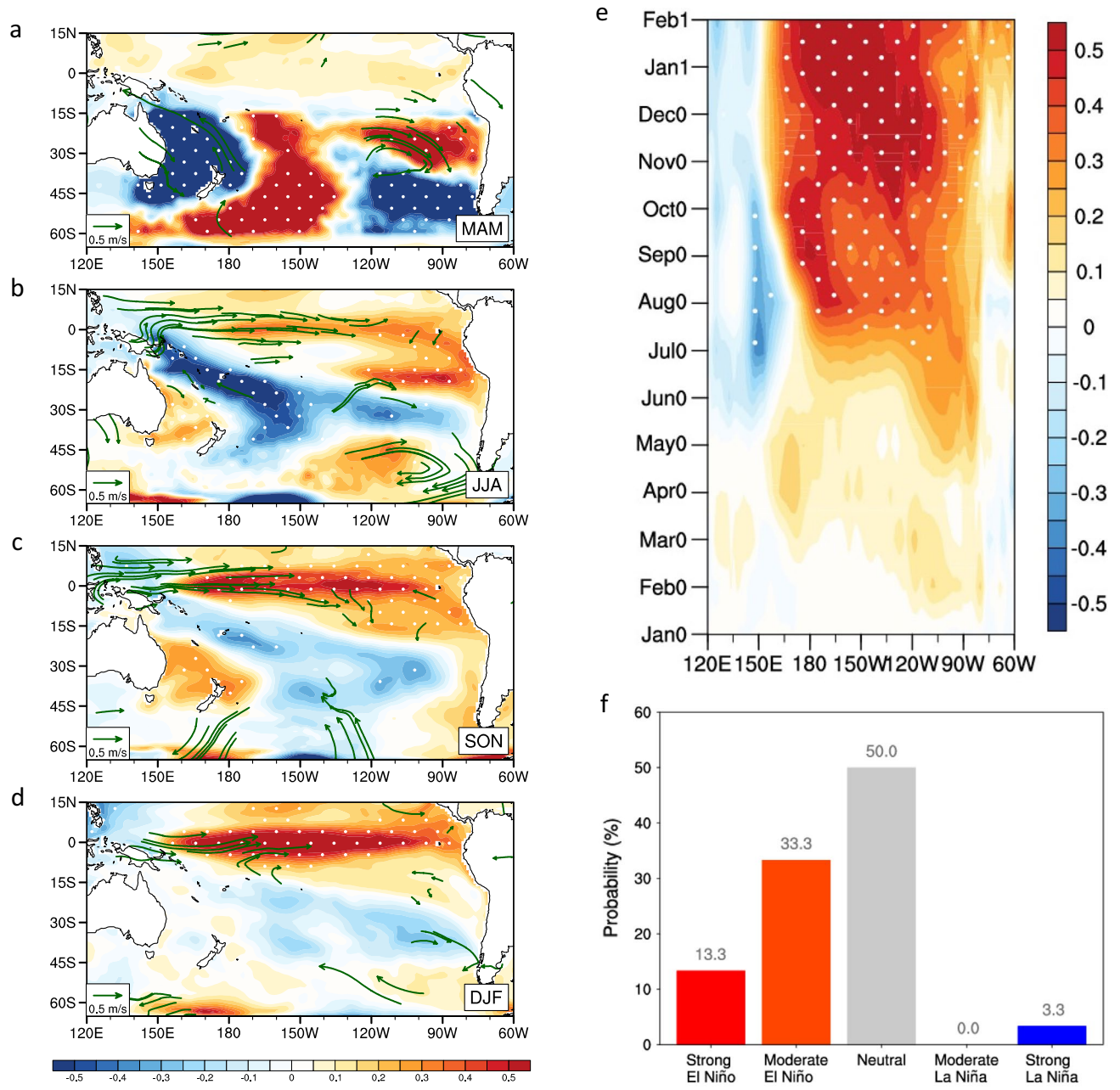

Fig. 10 **a**–**d** Ensemble-mean differences of SST (shading; °C) and 850 hPa winds (vector; m s^{-1}) between the SPQ-FORCE and CTRL simulations in **a** MAM0, **b** JJA0, **c** SON0, and **d** D0JF1. **e** Time-longitude plot of equatorial SSTAs (shading; °C) in the SPQ-FORCE compared to CTRL, averaged meridionally from 5°S to 5°N, from Jan0 to Feb1. **f** Probability distribution of ENSO events in the SPQ-FORCE simulation, categorizing strong El Niño, moderate El Niño, neutral, moderate La Niña, and strong La Niña. Numbers above the bars indicate the specific probability of the corresponding events. In (**a**–**e**), stippling highlights regions where values reach statistical significance at the 90% confidence level, and within (**a**–**d**), only wind vectors surpassing this confidence level are illustrated

in the experiment. Instead, it suggests that the emergence of an ENSO event here is more likely a result of the SPQ. Within the initiation phase of the South Pacific, a salient quadrupole-like SSTA configuration corresponding to SPQ manifests, along with noticeable southeasterly and northwesterly anomalies in the respective southwest and southeast Pacific regions. This configuration of SST and wind anomalies is favorable for WES feedback, that is, the anomalous southeasterly (northwesterly) in the southwest (southeast) Pacific strengthen (weaken) the background southeasterly trade wind, thereby enhancing (diminishing) the evaporation process, which in turn cools (heats) the seawater to the east (west) off Australia (Chile). During the following JJA0 season, South Pacific SSTAs begin to extend

into the tropical Pacific. This extension is facilitated through WES feedback. Over time, the contrasting negative and positive SSTAs in the western and in the central-eastern equatorial Pacific emerge, these anomalies lead to an energized gradient in the SST across the western-central Pacific. This SST gradient further generates and strengthens the westerly anomalies over the western equatorial Pacific. The anomalous westerlies then further induce warm ocean Kelvin wave that propagates eastward and downward. Consequently, by the ensuring winter, significant El Niño-like SSTAs surpassing 0.5 °C materialize within the equatorial Pacific.

To examine the equatorial Pacific SST evolution in details, Fig. 10e portrays the time-longitude illustration, contrasting the ensemble-mean SSTAs within the sensitivity experiments against the control experiments. From the onset in Jan0 through May0, the equatorial Pacific reveals no substantial warm SSTAs. While after Jun0, which marks the termination of prescribed SPQ-related SSTA forcing in the sensitivity simulation, noteworthy positive SSTAs begin to develop around 100°W in the eastern Pacific, complemented by the inception of negative SSTAs near 150°E. The warm equatorial SSTA center over the eastern Pacific then gradually develops westward and strengthens over time through Bjerknes feedback. During the D0JF1 season, coinciding with typical ENSO peak time, the maximum SSTAs position over 180–135°W. These simulated boreal winter SSTAs in the CESM align in magnitude and location with that in observation (Fig. 8d). While previous research emphasized the distinct role that precursors in the South Pacific play on the emergence of eastern Pacific (EP) El Niño (Ding et al. 2015a; You and Furtado 2017), the present analysis identifies a more pronounced affinity of SPQ with central Pacific (CP) El Niño (Ashok et al. 2007; Yu and Kao 2007; Kao and Yu 2009; Kug et al. 2009) both in observation and simulation. This distinction underscores the potentially unique contribution of SPQ in ENSO forecasting, particularly under the recent scenario that the CP El Niño happened more and more frequently (Gan et al. 2023).

Apart from analyzing ensemble-mean results, we also analyzed the 30 individual ensemble members to see the probability of a positive SPQ in inducing an El Niño. Events were categorized according to the Niño3.4 index as follows: neutral events (within ± 0.5 °C), moderate El Niño events (exceeding 0.5 °C but less than 1 °C), strong El Niño events (exceeding1°C), moderate La Niña events (below –0.5 °C but greater than –1 °C), and strong La Niña events (below –1 °C) (Fig. 10f). Within the 30 members analyzed, strong El Niño events constitute 13.3% of occurrences, and moderate El Niño events account for 33.3%. This significant change from 30 neutral events to 14 El Niño events indicates a 46.6% probability of SPQ catalyzing a shift from what might typically result in a neutral occurrence into an El Niño event. These findings, in alignment with existing observational analysis, further highlight the pivotal role that the boreal spring extratropical SPQ plays in the genesis of ensuring winter tropical ENSO.

4 Summary and discussion

In the present research, through observational analyses and numerical model experiments, we identified bidirectional influences between ENSO and the atmospheric (SPO) and oceanic (SPQ) variability modes, both situated within the South Pacific. We proved with forced model experiments that central tropical Pacific SSTAs associated with ENSO events can produce a teleconnection to the Southern Hemisphere to compete with atmospheric internal variability to control the formation of the SPO. We were able to show that the ENSO forcing, and the atmospheric internal dynamics are equally important and have comparable contribution to the interannual variability of the SPO. We next demonstrated that the atmospheric SPO can later trigger a SPQ event one month later. With a SPQ-related SSTA forcing experiment, we verified that the SPQ can evolve equatorward via the WES feedback mechanism and help give rise to an ENSO event. In addition, we should point out here that the significant role of SPQ in the development of ENSO does not deny the important role of tropical Pacific precursors, which are definitely important parts in ENSO forecast operation (DiNezio et al. 2017).

In the pursuit of enhancing ENSO prediction, a broader examination of climate modes from other oceans is warranted. Distinct phenomena, exemplified by the Indian Ocean Dipole (IOD; Saji et al. 1999), along with the dynamics within North Tropical Atlantic (NTA), are also recognized as potential ENSO precursors (Ham et al. 2013; Wang et al. 2017). Nonetheless, positive phases of the IOD and the NTA typically manifest a negative correlation with the ensuing year ENSO. This means that when the IOD and NTA are in their positive phases, they often promote the onset of ensuing La Niña events, even though these positive phases frequently coincide with El Niño occurrences. Such dynamics suggest that the IOD and NTA act as transitional agents, having the capacity to trigger single-year ENSO events. Contrastingly, the positive phase of the SPO and SPQ examined in this study, while also concurrent with El Niño events, exhibits a positive correlation with ENSO in the following year, which predisposes the climatic system to a subsequent El Niño. This relationship highlights the distinctive character of SPO/SPQ compared to other known ENSO precursors. Unlike the IOD and NTA, SPO/SPQ's behavior suggests an inherent capability to sustain, rather than merely transition, ENSO events. Consequently, the unique attributes of SPO/SPQ make it conducive to the development of multi-year ENSO events. This two-way influences between

ENSO and SPO/SPQ provide a new perspective to understand ENSO complexity. These connections could also help us better predict how ENSO will act under climate changes. These are important scientific questions that merit further investigation.

Author contributions RQD and XML designed the research framework. XML conducted data analyses and model experiments, plotted figures, and wrote the manuscript. YHT helped solve the problems in model experiments. JYY revised the manuscript and provided constructive suggestions. XFX reviewed and modified the manuscript.

Funding This work was supported by National Natural Science Foundation of China (42225501, 41975070) and Postgraduate Research and Practice Innovation Program of Jiangsu Province (KYCX21_0945).

Data availability All data used in this study are available in public repositories. The HadISST data are available at https://www.metoffice.gov.uk/hadobs/hadisst/data/download.html, the NCEP-NCAR reanalysis 1 data are available at https://psl.noaa.gov/data/gridded/data.ncep.reanalysis.html, and the CMAP precipitation data are available at https://psl.noaa.gov/data/gridded/data.cmap.html. The outputs from model simulations are available to readers upon request.

Declarations

Conflict of interest The authors declare no potential conflicts of interest.

References

Anderson BT (2003) Tropical Pacific sea-surface temperatures and preceding sea level pressure anomalies in the subtropical North Pacific. J Geophys Res Atmosph. https://doi.org/10.1029/2003JD003805

Anderson BT (2004) Investigation of a large-scale mode of ocean-atmosphere variability and its relation to tropical pacific sea surface temperature anomalies. J Clim 17:4089–4098. https://doi.org/10.1175/1520-0442(2004)017%3c4089:IOALMO%3e2.0.CO;2

Anderson BT, Perez RC, Karspeck A (2013) Triggering of El Niño onset through trade wind–induced charging of the equatorial Pacific. Geophys Res Lett 40:1212–1216. https://doi.org/10.1002/grl.50200

Ashok K, Behera SK, Rao SA et al (2007) El Niño Modoki and its possible teleconnection. J Geophys Res Oceans. https://doi.org/10.1029/2006JC003798

Bjerknes J (1969) Atmosppheric teleconnections from the equatorial Pacific atmospheric. Mon Weather Rev 97:163–172. https://doi.org/10.1175/1520-0493(1969)097%3c0163:ATFTEP%3e2.3.CO;2

Bond NA, Overland JE, Spillane M, Stabeno P (2003) Recent shifts in the state of the North Pacific. Geophys Res Lett. https://doi.org/10.1029/2003GL018597

Chang P, Zhang L, Saravanan R et al (2007) Pacific meridional mode and El Niño—Southern Oscillation. Geophys Res Lett. https://doi.org/10.1029/2007GL030302

Chiang JCH, Vimont DJ (2004) Analogous Pacific and Atlantic meridional modes of tropical atmosphere-ocean variability. J Clim 17:4143–4158. https://doi.org/10.1175/JCLI4953.1

Delworth TL, Broccoli AJ, Rosati A et al (2006) GFDL's CM2 global coupled climate models. Part I: formulation and simulation characteristics. J Clim 19:643–674. https://doi.org/10.1175/JCLI3629.1

DiNezio PN, Deser C, Okumura Y, Karspeck A (2017) Predictability of 2-year La Niña events in a coupled general circulation model. Clim Dyn 49:4237–4261. https://doi.org/10.1007/s00382-017-3575-3

Ding R, Li J, Tseng Y et al (2015a) The Victoria mode in the North Pacific linking extratropical sea level pressure variations to ENSO. J Geophys Res Atmos 120:27–45. https://doi.org/10.1002/2014JD022221

Ding R, Li J, Tseng Y (2015b) The impact of South Pacific extratropical forcing on ENSO and comparisons with the North Pacific. Clim Dyn 44:2017–2034. https://doi.org/10.1007/s00382-014-2303-5

Ding R, Li J, Tseng Y et al (2017) Joint impact of North and South Pacific extratropical atmospheric variability on the onset of ENSO events: NORTH AND SOUTH PACIFIC IMPACT ON ENSO. J Geophys Res Atmos 122:279–298. https://doi.org/10.1002/2016JD025502

Ding R, Li J, Yang R et al (2020) On the differences between the south pacific meridional and quadrupole modes. J Geophys Res Oceans. https://doi.org/10.1029/2019JC015500

Fedorov AV, Hu S, Lengaigne M, Guilyardi E (2015) The impact of westerly wind bursts and ocean initial state on the development, and diversity of El Niño events. Clim Dyn 44:1381–1401. https://doi.org/10.1007/s00382-014-2126-4

Gan R, Liu Q, Huang G et al (2023) Greenhouse warming and internal variability increase extreme and central Pacific El Niño frequency since 1980. Nat Commun 14:394. https://doi.org/10.1038/s41467-023-36053-7

Ham Y-G, Kug J-S, Park J-Y, Jin F-F (2013) Sea surface temperature in the north tropical Atlantic as a trigger for El Niño/Southern Oscillation events. Nature Geosci 6:112–116. https://doi.org/10.1038/ngeo1686

Hendon HH, Wheeler MC, Zhang C (2007) Seasonal dependence of the MJO–ENSO relationship. J Clim 20:531–543. https://doi.org/10.1175/JCLI4003.1

Hu Z-Z, Kumar A, Zhu J et al (2019) On the challenge for ENSO cycle prediction: an example from NCEP climate forecast system, version 2. J Clim 32:183–194. https://doi.org/10.1175/JCLI-D-18-0285.1

Hurrell JW, Holland MM, Gent PR et al (2013) The community earth system model: a framework for collaborative research. Bull Am Meteor Soc 94:1339–1360. https://doi.org/10.1175/BAMS-D-12-00121.1

Ineson S, Balmaseda MA, Davey MK et al (2018) Predicting El Niño in 2014 and 2015. Sci Rep 8:10733. https://doi.org/10.1038/s41598-018-29130-1

Jin F-F (1997a) An equatorial ocean recharge paradigm for ENSO. Part I: conceptual model. J Atmos Sci 54:811–829. https://doi.org/10.1175/1520-0469(1997)054%3c0811:AEORPF%3e2.0.CO;2

Jin F-F (1997b) An equatorial ocean recharge paradigm for ENSO. Part II: a stripped-down coupled model. J Atmos Sci 54:830–847. https://doi.org/10.1175/1520-0469(1997)054%3c0830:AEORPF%3e2.0.CO;2

Kalnay E, Kanamitsu M, Kistler R et al (1996) The NCEP/NCAR 40-year reanalysis project. Bull Am Meteor Soc 77:437–472. https://doi.org/10.1175/1520-0477(1996)077%3c0437:TNYRP%3e2.0.CO;2

Kao H-Y, Yu J-Y (2009) Contrasting Eastern-Pacific and Central-Pacific types of ENSO. J Clim 22:615–632. https://doi.org/10.1175/2008JCLI2309.1

Kug J-S, Jin F-F, An S-I (2009) Two types of El Niño events: cold tongue El Niño and warm pool El Niño. J Clim 22:1499–1515. https://doi.org/10.1175/2008JCLI2624.1

Le T, Bae D-H (2019) Causal links on interannual timescale between ENSO and the IOD in CMIP5 future simulations. Geophys Res Lett 46:2820–2828. https://doi.org/10.1029/2018GL081633

Li X, Zhang W, Ding R, Shi L (2020) Joint impact of North Pacific Victoria mode and South Pacific Quadrapole mode on Pacific ITCZ summer precipitation. Clim Dyn 54:4545–4561. https://doi.org/10.1007/s00382-020-05243-0

Madden RA, Julian PR (1994) Observations of the 40–50-day tropical oscillation—a review. Mon Weather Rev 122:814–837. https://doi.org/10.1175/1520-0493(1994)122%3c0814:OOTDTO%3e2.0.CO;2

McPhaden MJ, Bahr F, Du Penhoat Y et al (1992) The response of the western equatorial Pacific Ocean to westerly wind bursts during November 1989 to January 1990. J Geophys Res Oceans 97:14289–14303. https://doi.org/10.1029/92JC01197

McPhaden MJ, Zebiak SE, Glantz MH (2006) ENSO as an integrating concept in earth science. Science 314:1740–1745. https://doi.org/10.1126/science.1132588

Min Q, Zhang R (2020) The contribution of boreal spring south pacific atmospheric variability to El Niño occurrence. J Clim 33:8301–8313. https://doi.org/10.1175/JCLI-D-20-0122.1

Mo KC, Higgins RW (1998) The Pacific-South American modes and tropical convection during the Southern Hemisphere Winter. Mon Wea Rev 126:1581–1596. https://doi.org/10.1175/1520-0493(1998)126%3c1581:TPSAMA%3e2.0.CO;2

Rayner NAA, Parker DE, Horton EB et al (2003) Global analyses of sea surface temperature, sea ice, and night marine air temperature since the late nineteenth century. J Geophys Res Atmosph. https://doi.org/10.1029/2002JD002670

Rogers JC (1981) The North Pacific oscillation. J Climatol 1:39–57. https://doi.org/10.1002/joc.3370010106

Saji NH, Goswami BN, Vinayachandran PN, Yamagata T (1999) A dipole mode in the tropical Indian Ocean. Nature 401:360–363. https://doi.org/10.1038/43854

Tang Y, Zhang R-H, Liu T et al (2018) Progress in ENSO prediction and predictability study. Natl Sci Rev 5:826–839. https://doi.org/10.1093/nsr/nwy105

Timmermann A, An S-I, Kug J-S et al (2018) El Niño-Southern oscillation complexity. Nature 559:535–545. https://doi.org/10.1038/s41586-018-0252-6

Tseng Y, Hu Z-Z, Ding R, Chen H (2017) An ENSO prediction approach based on ocean conditions and ocean–atmosphere coupling. Clim Dyn 48:2025–2044. https://doi.org/10.1007/s00382-016-3188-2

Vimont DJ, Battisti DS, Hirst AC (2001) Footprinting: a seasonal connection between the tropics and mid-latitudes. Geophys Res Lett 28:3923–3926. https://doi.org/10.1029/2001GL013435

Vimont DJ, Battisti DS, Hirst AC (2003a) The seasonal footprinting mechanism in the CSIRO general circulation models. J Clim 16:2653–2667. https://doi.org/10.1175/1520-0442(2003)016%3c2653:TSFMIT%3e2.0.CO;2

Vimont DJ, Wallace JM, Battisti DS (2003b) The seasonal footprinting mechanism in the pacific: implications for ENSO. J Clim 16:2668–2675. https://doi.org/10.1175/1520-0442(2003)016%3c2668:TSFMIT%3e2.0.CO;2

Wang L, Yu J-Y, Paek H (2017) Enhanced biennial variability in the Pacific due to Atlantic capacitor effect. Nat Commun 8:14887. https://doi.org/10.1038/ncomms14887

Wieners CE, Dijkstra HA, de Ruijter WPM (2019) The interaction between the Western Indian Ocean and ENSO in CESM. Clim Dyn 52:5153–5172. https://doi.org/10.1007/s00382-018-4438-2

Xie P, Arkin PA (1997) Global precipitation: a 17-year monthly analysis based on gauge observations, satellite estimates, and numerical model outputs. Bull Am Meteor Soc 78:2539–2558. https://doi.org/10.1175/1520-0477(1997)078%3c2539:GPAYMA%3e2.0.CO;2

Xie S, Philander SGH (1994) A coupled ocean-atmosphere model of relevance to the ITCZ in the eastern Pacific. Tellus A 46:340–350

You Y, Furtado JC (2017) The role of South Pacific atmospheric variability in the development of different types of ENSO. Geophys Res Lett 44:7438–7446. https://doi.org/10.1002/2017GL073475

You Y, Furtado JC (2019) The relationship between South Pacific atmospheric internal variability and ENSO in the North American multimodel ensemble phase-II models. Geophys Res Lett 46:12398–12407. https://doi.org/10.1029/2019GL084637

Yu J-Y, Kao H-Y (2007) Decadal changes of ENSO persistence barrier in SST and ocean heat content indices: 1958–2001. J Geophys Res Atmosph. https://doi.org/10.1029/2006JD007654

Zhang H, Clement A, Di Nezio P (2014) The South Pacific meridional mode: a mechanism for ENSO-like variability. J Clim 27:769–783. https://doi.org/10.1175/JCLI-D-13-00082.1

Zheng J, Wang F (2017) On the formation of the South Pacific quadrupole mode. Theor Appl Climatol 130:331–344. https://doi.org/10.1007/s00704-016-1885-8

Zhu J, Kumar A, Huang B et al (2016) The role of off-equatorial surface temperature anomalies in the 2014 El Niño prediction. Sci Rep 6:19677. https://doi.org/10.1038/srep19677